High-order harmonic generation by a driven mesoscopic ring with a localized impurity

N. F. Hinsche,* A. S. Moskalenko,† and J. Berakdar
Institut für Physik, Martin-Luther-Universität Halle-Wittenberg, Halle 06120, Germany
(Received 8 October 2008; published 19 February 2009)

We investigate theoretically the electron dynamics in a single-channel mesoscopic ring with a localized impurity subjected to picosecond linearly polarized asymmetric electromagnetic pulses. A nonequilibrium coherent population of electronic states that possesses a time-dependent polarization is induced. The associated radiation emission decays on a time scale determined by the system relaxation and hence lasts long after the pulses have perished. We derive analytically and confirm numerically that the presence of an impurity influences strongly the time-dependent charge polarization and allows the generation of higher harmonics in the terahertz range.

DOI: 10.1103/PhysRevA.79.023822 PACS number(s): 42.65.Ky, 78.67.−n, 42.65.Re, 72.10.Fk

I. INTRODUCTION

In a seminal work [1,2] Aharonov and Bohm predicted in 1959 that the partial waves of charged particles are influenced by the presence of a vector potential and experience a phase shift even in regions where electromagnetic fields are absent. This phenomenon known as the Aharonov-Bohm effect [3] leads in phase-coherent rings to the existence of a persistent (*equilibrium*) current [4–8]. Over the past two decades various aspects of the electronic properties of nanoscopic and mesoscopic rings (MRs) (role of disorder, electronic correlations, etc.) have been investigated both theoretically and experimentally [7–19]. Another aspect which gained much attention recently is the *nonequilibrium* charge dynamics in MRs driven by time-dependent electromagnetic fields [20–26]. The generation of nonequilibrium currents and time-dependent charge-density oscillations was predicted. Associated with the latter is the emission of light with characteristics determined by the ring properties and the driving fields [10,21,27–29]. The question we pose here is the possibility for utilizing MRs as a versatile source for the generation of higher harmonics, a topic of much importance for optical spectroscopy and lasers developments [30–35]. The system we inspect is a ballistic MR with a localized impurity driven by linearly polarized half-cycle electromagnetic pulses (HCPs). A HCP is in fact a monocycle pulse with a short but strong half cycle with duration τ_p, followed by a weak but long second half cycle of opposite polarity [see Fig. 1(b)] (long or short is meant in comparison to the electron round-trip time τ_F which is in the range of picoseconds). Currently available HCPs possess half-cycle durations τ_p below 1 ps and peak field amplitudes of up to several hundreds of kV/cm [36–38]. For τ_F being longer than τ_p the *impulsive approximation* (IA) [20,29,39,40] becomes applicable and the action of a HCP can be subsumed in an *instantaneous momentum kick* $\boldsymbol{p}=q\int_0^{\tau_p}\boldsymbol{F}(t)dt$. Here $\boldsymbol{F}$ is the electric field amplitude of the pulse and q is the carrier charge (the pulse is applied at $t=0$). As shown previously [21,29], HCP applied to MR generates a postpulse time-dependent electric polarization with an emission spectrum containing multiple fundamental harmonics $\omega_0=\frac{N}{4}\Omega_0$ with $\Omega_0=\hbar/(m^*\rho_0^2)$ [41], where ρ_0 and m^* are the ring radius and the electron effective mass and N is the number of electrons. If the ring contains an impurity, e.g., experimentally realized in Ref. [42] by cutting the ring at one position, one may expect the introduction of additional channels for the charge radiative decay and hence additional frequencies. This is the intuitive picture we wish to explore quantitatively—a task which, to our knowledge, has not been addressed before. We find that under appropriate conditions the presence of the localized impurity results in additional higher harmonics with frequencies in the terahertz range.

II. POSTPULSE ELECTRON DYNAMICS

The system under study is an isolated ballistic ring at low temperature ($T\approx 0$ K). If the ring thickness and width are smaller than the Fermi wavelength λ_F (a condition routinely realizable by present day technology), the consideration can be restricted to the lowest radial channel. Accounting for additional radial channels can be done as in Ref. [20]. The ring is subjected at the time $t_1=0$ to a single HCP. Within the IA the time-dependent single-particle wave function Ψ obeys then the following time-dependent Schrödinger equation (TDSE):

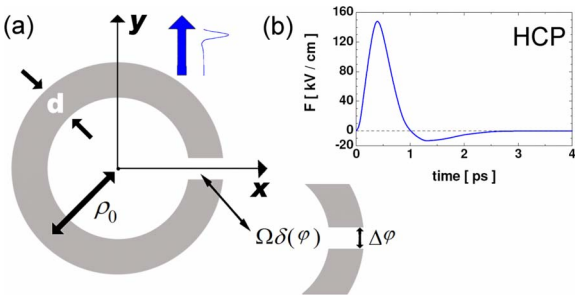

FIG. 1. (Color online) (a) Schematic drawing of the MR. (b) HCP as reported in [36].

*Also at Forschungszentrum Dresden-Rossendorf, Abteilung Halbleitermaterialien, 01328 Dresden, Germany.

†Also at A. F. Ioffe Physico-Technical Institute, 194021 St. Petersburg, Russia. andrey.moskalenko@physik.uni-halle.de

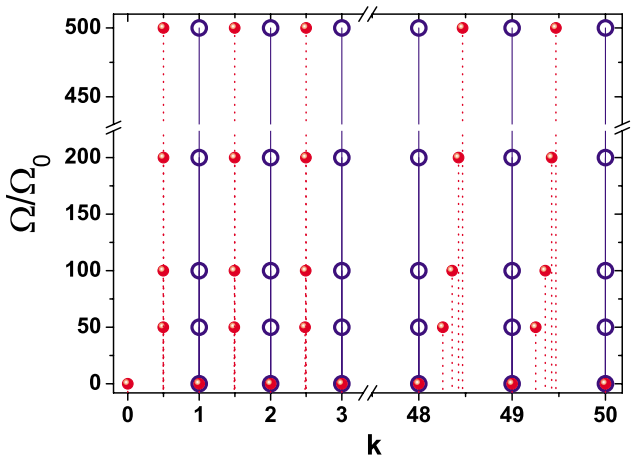

FIG. 2. (Color online) Quantum numbers k as a function of the potential strength Ω measured in units $\Omega_0=\frac{\hbar^2}{m^*\rho_0^2}$. Shown are the energies of even-parity (full dots) and odd-parity (open circles) stationary eigenfunctions [Eqs. (4) and (5)].

$$i\hbar\frac{\partial\Psi}{\partial t}=\left[-\frac{\hbar^2}{2m^*\rho_0^2}\frac{\partial^2}{\partial\varphi^2}+V_{\rm int}(\varphi,t)+V_{\rm imp}(\varphi)\right]\Psi, \quad (1)$$

where

$$V_{\rm int}(\varphi,t)=-\rho_0 p\,\delta(t-t_1)\sin\varphi. \quad (2)$$

Here the linear polarization vector of the pulse defines the y axis and m^* is the effective mass of the particle. If the localized impurity acts within a region smaller than λ_F then its potential can be modeled by

$$V_{\rm imp}(\varphi)=\Omega\,\delta(\varphi), \quad (3)$$

where the strength Ω is measured in units of energy per angle interval and the angle φ is counted from the location of the impurity. A realization of this situation is a small cut in a ring or an inclusion of a material with a broader band gap.

The stationary states of the field-free case read

$$\psi_k(\varphi)=\begin{cases}\frac{1}{\sqrt{\pi}}\sin(k\varphi), & k\in\mathbb{Z}\\ \left(\pi+\frac{\sin(2k\pi)}{2k}\right)^{-1/2}\cos[k(\varphi-\pi)], & k\in\mathbb{R},\end{cases} \quad (4)$$

where the eigenenergies $E=\frac{\hbar^2k^2}{2m^*}$ are determined by

$$\cos(2\pi k)+\frac{\Omega m^*\rho_0^2}{k\hbar^2}\sin(2\pi k)=1. \quad (5)$$

Due to the presence of the impurity half of the k values that belong to the even-parity stationary eigenfunctions ψ_k become a noninteger (shown as full spheres in Fig. 2). States with odd parity are not affected as they have a node at $\varphi=0$. Their quantum numbers k remain an integer (shown as open circles in Fig. 2). The spectrum is illustrated in Fig. 2. For particles with small energies in comparison with the impurity potential, a splitting of the energy levels (limited to the splitting of k values by 1/2) is observed. With an increasing particle energy the probability of the particle to transmit through the impurity potential increases and in the limit of high energies the particle is hardly affected by the impurity.

Obviously, the energy levels that allow additional state-to-state transitions are controllable by appropriately choosing the potential strength Ω. In what follows $\Psi_{k_0}(\varphi,t)$ denotes the time-dependent solution of the TDSE with the initial condition that the particle starts from the state characterized by quantum number $k=k_0$. $\Psi_{k_0}(\varphi,t)$ can be expanded in terms of the MR stationary eigenstates ψ_k as

$$\Psi_{k_0}(\varphi,t)=\sum_k C_{k,k_0}(t)\psi_k(\varphi)e^{-iE_kt/\hbar}. \quad (6)$$

For the particular case of HCP the solutions $\Psi_{k_0}(\varphi,t)$ satisfy the matching condition [29]

$$\Psi(\varphi,t=0^+)=\Psi(\varphi,t=0^-)e^{i\alpha\sin\varphi}, \quad (7)$$

where $t=0^-$ and $t=0^+$ refer to times shortly before and after the application of the electromagnetic pulse. The parameter α,

$$\alpha=\rho_0 p/\hbar,\quad \boldsymbol{p}=q\int_0^{\tau_p}\boldsymbol{F}(t)dt, \quad (8)$$

characterizes the action (normalized by $\hbar$) delivered to the ring by the HCP. From Eqs. (6) and (7) we infer for the expansion coefficients

$$C_{k,k_0}(t<0)=\delta_{k,k_0}, \quad (9)$$

$$C_{k,k_0}(t>0)=C_{k,k_0}^{i,j}, \quad (10)$$

where $\delta_{m,n}$ is the Kronecker symbol. The expressions for the coefficients $C_{k,k_0}^{i,j}$ are given in Appendix B; the superscript i,j determines the types of the initial and final states that can be either odd or even.

To characterize the charge distribution in the direction of the HCP we employ a parameter that stands for the localization of the single-particle probability density along the y axis,

$$\langle\sin\varphi\rangle_{k_0}(t)=\int_0^{2\pi}|\Psi_{k_0}(\varphi,t)|^2\sin\varphi d\varphi. \quad (11)$$

The corresponding (single-particle) dipole moment along the y axis is given by

$$\mu_{k_0,y}(t)=q\rho_0\langle\sin\varphi\rangle_{k_0}(t). \quad (12)$$

Analogously for the single-particle charge polarization along the x axis we define

$$\langle\cos\varphi\rangle_{k_0}(t)=\int_0^{2\pi}|\Psi_{k_0}(\varphi,t)|^2\cos\varphi d\varphi, \quad (13)$$

$$\mu_{k_0,x}(t)=q\rho_0\langle\cos\varphi\rangle_{k_0}(t). \quad (14)$$

The total dipole moment of the MR along the y axis (x axis) $\mu_{y(x)}(t)$ is

$$\mu_{y(x)}(t)=\sum_{k_0,\sigma}f_{k_0,\sigma}^0\mu_{k_0,y(x)}(t), \quad (15)$$

where $f_{k_0,\sigma}^0$ is the equilibrium distribution function and σ refer to the particle spin. By the pulse application, the charge

carriers are transferred into coherent excited states that propagate according to the field-free Hamiltonian. The coherences determine the dynamics of the dipole moment. However dissipative processes result in a loss of coherence, and therefore to a decay of the dipole moment. The physical processes behind this behavior are mainly electron-phonon scattering [21,43–45] and electron-electron interaction [46–48]. Here we assume the decay of the dipole moment to be characterized by a single time constant, which is the relaxation time τ_{rel}. The relaxation time τ_{rel} depends on the parameters of the MR; for low temperatures it can be even longer than 1 ns [21]. Equation (15) then reads

$$\mu_{y(x)}(t) = \mu_{y(x)}(t<0) + e^{-t/\tau_{\mathrm{rel}}}\Bigg[\sum_{k_0,\sigma} f^0_{k_0,\sigma}\mu_{k_0,y(x)}(t) - \mu_{y(x)}(t<0)\Bigg]. \tag{16}$$

The equilibrium dipole moment of the ring vanishes in absence of the impurity and otherwise it is finite and directed along y axis, i.e., $\mu_x(t<0)=0$ and $\mu_y(t<0)\neq 0$, if $\Omega\neq 0$.

III. EMISSION PROPERTIES

The pulse-induced dynamical charge polarization in a MR is associated with the emission of electromagnetic dipole radiation. We note that due to the fulfilled relations $\tau_p \ll \tau_F$ and $\tau_p \ll \tau_{\mathrm{rel}}$, the electromagnetic radiation is emitted mainly when the driving external electric field is already absent. The oscillating charge density decays within a time of the order of the relaxation time τ_{rel}. The oscillations can be sustained for a much longer time if a sequence of HCPs is applied [29]. It is even possible to influence the specific characteristics of the radiation spectrum by appropriately designing the sequence and shape of the HCPs. In such a way pulse-driven MRs can serve as an efficient and a controllable source of electromagnetic radiation. The intensity of the emitted radiation depends on time. Here the time-integrated emission spectrum is calculated (the time-dependent emission spectrum is beyond the scope of this work and is discussed in Ref. [44]). The main contribution to the emission spectrum is determined by the dipole contribution to the emitted electric field being proportional to the second derivative of the dipole moment of the MR. Therefore, the emission spectrum up to a normalization factor is given by

$$I(\omega) \propto [|\ddot{\mu}_y(\omega)|^2 + |\ddot{\mu}_x(\omega)|^2], \tag{17}$$

where $\ddot{\mu}_y(\omega)$ and $\ddot{\mu}_x(\omega)$ denote the Fourier-transformed second time derivatives $\ddot{\mu}_y(t)$ and $\ddot{\mu}_x(t)$, respectively.

In our numerical calculations we assume $\tau_{\mathrm{rel}}=1$ ns, which is long enough to resolve different harmonics. Shorter (longer) times will lead to the broadening (narrowing) of the peaks in the emission spectrum.

IV. NUMERICAL RESULTS

For our numerical calculations of the dipole moment dynamics and the emission spectra given by Eqs. (16) and (17), we used the parameters of electrons in a GaAs quantum ring. The ring radius is $\rho_0=132$ nm (as in the experiment of Ref. [8]) and the electron effective mass is $m^*=0.067m_0$, where m_0 is the free electron mass. Our ring contains $N=20$ electrons and the width of the ring is small enough for the single-channel model to be valid. We employ HCPs with a sine-square shape having a time duration of $\tau_p=1$ ps and linearly polarized along the y axis. The duration of the HCP and the sine-square shape of the pulse determines the relation between the parameter α and the peak value of electric field [see Eq. (8)]. The case where the HCP is linearly polarized along the x axis is discussed in Sec. V and in Appendix A. As outlined above, the action of the pulse is characterized by the parameter α. Hence, in the numerical illustrations below we provide only the single parameter α that contains all relevant external field properties. For modeling relaxation processes of the electronic system we used a phenomenological relaxation time $\tau_{\mathrm{rel}}=1$ ns. With these parameters and assumptions we calculated the dynamics of the HCP-induced time-dependent charge polarization of the ring and the corresponding emission spectrum for different pulse and impurity potential strengths.

The time dependencies of the electric dipole along the y axis $\mu_y(t)$ induced by a weak HCP of strength $\alpha=0.1$ (this corresponds to a peak value of electric field $F=10$ V/cm) are shown in the left panel of Fig. 3. The impurity barrier strength Ω is increased from 0 meV in (a) to 0.5 meV in (b) and 10 meV in (c). One can see that in the case of such a weak excitation the dynamics of the dipole moment demonstrates beatings [21,29] in the absence of impurity. The amplitude of the beatings is decreasing on a time scale much larger than the oscillation period due to the relaxation. In the presence of impurity the dynamics of $\mu_y(t)$ is evidently a result of composition of more than two harmonics. In the case of weak excitations the dynamics of the dipole moment is determined by generated coherences between the states near the Fermi level and the corresponding transition matrix elements. In the case of $\mu_y(t)$ the transition matrix elements $\langle\phi_{k'}|\sin\varphi|\phi_k\rangle$ [cf. Eqs. (6), (11), and (12)] are different from zero only for transitions between the states of different parity. The expression for these matrix elements is given in Appendix A. Possible transitions are illustrated in Fig. 4 for $N=0 \pmod 4$ electrons in the ring. All other transitions, which are not shown in Fig. 4, do not contribute to the dynamics because either the generated coherences are small or the corresponding matrix elements are vanishing or small. Figure 4(a) corresponds to the case without impurity. We clearly see that two close frequencies should be present in the dipole moment dynamics. When the impurity barrier is introduced other transitions start to contribute more to the dynamics. The case of a very high impurity barrier is depicted in Fig. 4(b) where three transitions with close frequencies, which are approximately 1.5 times larger than the frequencies for the perfect ring case (they are around $\omega_0 = 2\pi/\tau_F = \frac{N\hbar}{4m^*\rho_0^2}$), and one transition with a frequency, which is approximately a half of the frequencies in absence of impurity, should give the strongest contributions to the dynamics of the dipole moment. This is confirmed by the corresponding emission spectra shown in the left panel of Fig. 5. In Fig. 5(c) the contribution with the frequency around $\omega_0/2$

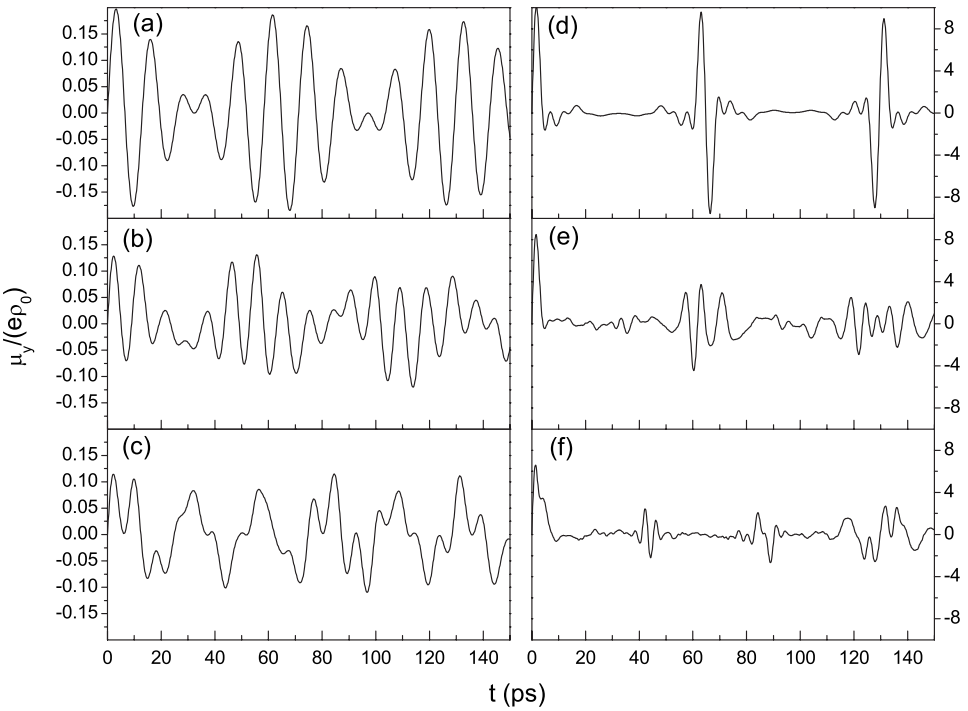

FIG. 3. Time dependence of the generated electric dipole moment along the y axis μ_y for varying impurity potential strengths Ω and two different strengths (weak and strong) of the HCP α. (a) $\alpha=0.1$ ($F=10$ V/cm), $\Omega=0$; (b) $\alpha=0.1$, $\Omega=0.5$ meV; (c) $\alpha=0.1$, $\Omega=10$ meV; (d) $\alpha=10$ ($F=1$ kV/cm), $\Omega=0$; (e) $\alpha=10$, $\Omega=0.5$ meV; (f) $\alpha=10$, $\Omega=10$ meV.

is small but still visible. Increase in the impurity potential beyond $\Omega=10$ meV does not lead to any significant changes in the dipole moment dynamics and the emission spectrum. The energy barrier can be considered as infinite. In the case of weak excitations the dynamical part of the dipole moment along the x axis $\mu_x(t)$ is negligibly small.

The time dependencies of the electric dipole along the y axis $\mu_y(t)$ induced by a strong HCP of strength $\alpha=10$ ($F=1$ kV/cm) are shown in the right panel of Fig. 3. The impurity barrier strength Ω is increased from 0 meV in (d) to 0.5 meV in (e) and 10 meV in (f). The strong pulse creates populations far from the Fermi level as well as coherences between distant levels. In the absence of impurity the transition matrix elements are nonvanishing only for transitions between neighboring levels. Therefore, the dynamics of $\mu_y(t)$ is governed by many harmonics with close frequencies. There are no contributions from coherences between distant levels. This results into a typical dynamics of revivals and collapses as in Ref. [21] (where, however, it was a result of a nonzero temperature creating equilibrium population of distant levels). The corresponding spectrum is shown in Fig. 5(d). With respect to the case of weak excitations the spectrum maximum is blueshifted. This is a result of the energy transfer from the HCP to the MR, which is connected with the momentum transfer. The shift scales quadratically with the HCP strength [29]. One can also notice that the emission intensity increases dramatically with increasing the excitation strength. By increasing the impurity potential the dynamics of the dipole moment becomes more irregular as evident from Figs. 3(e) and 3(f). Coherences between distant levels start to contribute to the dipole moment dynamics due to an increase in the transition matrix elements [Eq. (A5)]. The maximum of the emission intensity is additionally shifted toward the blue region [see Figs. 5(e) and 5(f)]. Apart from this shift one can resolve more high harmonics far away from the emission maximum. This is seen in Fig. 6. It is important to remark that the scale is kept the same in all panels of Figs. 5 and 6. For $\Omega=0.5$ meV frequencies up to around $28\omega_0$ are present. For $\Omega=10$ meV and larger impurity barrier frequencies up to around $35\omega_0$ can be resolved

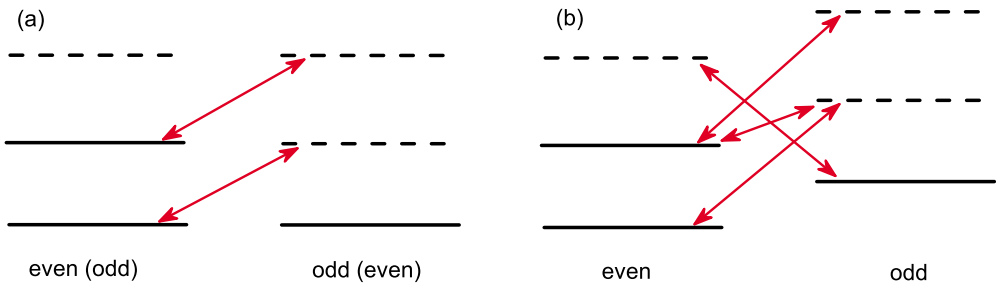

FIG. 4. (Color online) Scheme of transitions responsible for the dynamics of $\mu_y(t)$ (shown by arrows) in the case of weak excitations. Panel (a) corresponds to the case of no impurity whereas panel (b) corresponds to the case of a high impurity barrier. Only the levels near the Fermi level are shown. Full lines indicate the levels filled before the excitation and dashed lines indicate the empty levels for $N=0$ (mod 4) electrons in the MR at zero temperature. Notations "odd" or "even" relate to the symmetry of the wave functions of the shown levels.

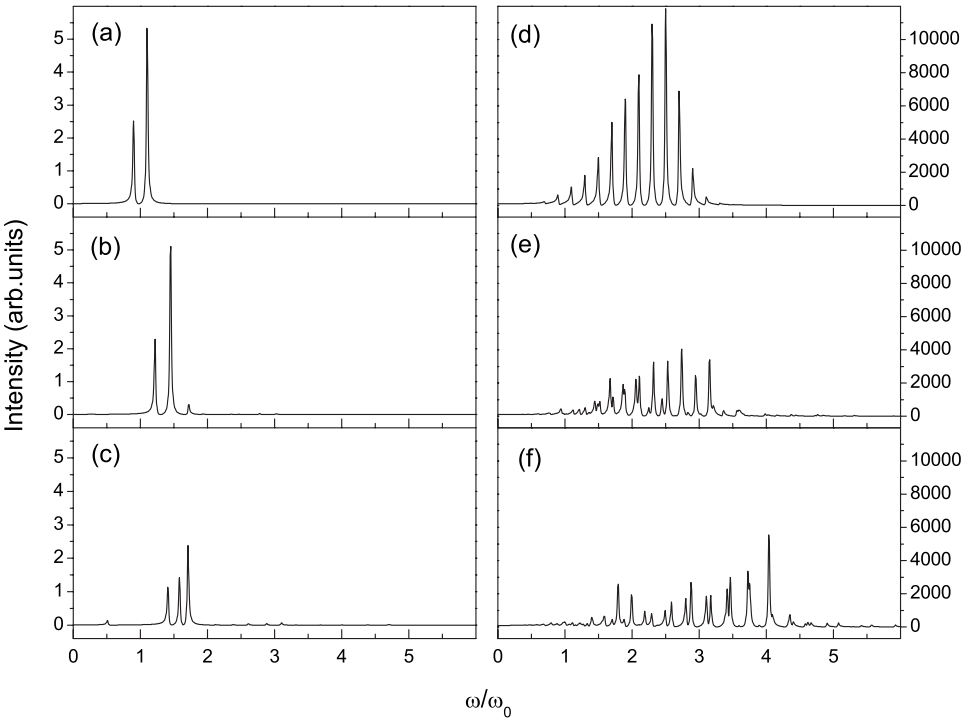

FIG. 5. Emission intensity $I(\omega)$ for varying impurity potential strengths Ω and two different strengths (weak and strong) of the HCP α: (a) $\alpha=0.1$ ($F=10$ V/cm), $\Omega=0$; (b) $\alpha=0.1$, $\Omega=0.5$ meV; (c) $\alpha=0.1$, $\Omega=10$ meV; (d) $\alpha=10$ ($F=1$ kV/cm), $\Omega=0$; (e) $\alpha=10$, $\Omega=0.5$ meV; (f) $\alpha=10$, $\Omega=10$ meV. The frequency ω is normalized by $\omega_0=\frac{N\hbar}{4m^*\rho_0^2}$ (which corresponds to approximately 0.08 THz for the parameters of the MR used here).

which corresponds approximately to 3 THz. The magnitudes of the high-frequency components of the emission spectrum are much smaller than the magnitudes of the low-frequency components but comparable with those of the MR driven by a weak HCP with $\alpha=0.1$. The emitted intensity can be strongly increased by using a planar array of MRs such as the configuration experimentally realized in Ref. [42]. A further increase in the excitation field strength leads to a violation of an assumption of pretty long relaxation times when the average energy gained by an electron from the HCP $\frac{\alpha^2}{4}\Omega_0$ [29] reaches the energy of the LO phonon in GaAs, which is 36 meV. For the chosen ring parameters this sets a limit $\alpha<60$.

In the case of a strongly driven ring with a large impurity barrier, a considerable dynamical part of the dipole moment along the x axis $\mu_x(t)$ is generated. However it contributes only to the low-frequency range of the spectrum. The reasons are similar to those discussed in Appendix A. In Fig. 5(f) the emission generated in the frequency range below $2\omega_0$ comes mostly from $\mu_x(t)$. We have also made calculations for a larger number of electrons in the MR. The conclusions are similar to those discussed above. By changing the parameters of the MR and the number of electrons the properties of emission can be adjusted.

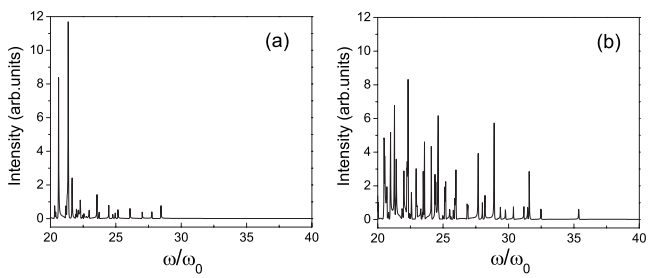

FIG. 6. High-frequency range of the emission spectra. (a) corresponds to Fig. 5(e) and (b) corresponds to Fig. 5(f).

V. CONCLUSION

Summarizing, when a single-channel ballistic mesoscopic ring containing a localized impurity is exposed to a single linearly polarized half-cycle pulse, the induced time-dependent charge oscillations and the resulting radiation emission are influenced strongly by the potential barrier of the impurity. A controlled generation of high harmonics can be achieved for strong excitations and high impurity barriers if the pulse polarization axis is perpendicular to the line connecting the ring center and the impurity. Planar or three-dimensional arrays of such driven mesoscopic rings could be potentially used for terahertz spectroscopic studies. With respect to a practical realization of a terahertz-emitting device based on the arrays of cut rings, it should be noticed that particular device properties would strongly depend on the number N of rings in the array, the chosen geometry, and optical system. As far as the radiation is coherent, the emitted intensity would scale as N^2 up to some limit, where the absorption of the energy of HCP pulses in the ring array becomes significant. The spatial coherence of the emitted terahertz radiation would strongly depend on the setup used for filtering out high-order harmonics that can be based on a terahertz photonic crystal [49]. Our estimation shows that the power of the terahertz radiation emitted from a single ring can be on the order of 10^{-20} W [e.g., for the parameters of Fig. 6(b)]. Taking an array of 10^9 rings we obtain a power on the order of some milliwatts.

In a high symmetry case where the pulse electric field is linearly polarized parallel to the line connecting the ring center and the impurity, we observe only marginal modifications

of the emission spectrum with respect to the perfect ring case (cf. Appendix A). This finding can be used to determine the position of a localized defect by monitoring the emission spectrum and rotating the polarization axis of the pulse. Finally we note that similar arguments as in the recollision model [30,33] apply for the interpretation of the demonstrated effect. Electrons excited by an electromagnetic pulse bounce off the impurity producing coherent light bursts. The difference to the conventional recollision model is that in our system the role of the ionic potential of the core atom [51] is played by the localized impurity potential and the recollisions are forced not by the periodicity of the exciting field but by the ring geometry.

APPENDIX A: HCP LINEARLY POLARIZED ALONG THE *x* AXIS

The interaction of the electrons in the ring with a HCP linearly polarized along the x axis Eq. (2) is

$$V_{\mathrm{int}}(\varphi,t) = -\rho_0 p\,\delta(t-t_1)\cos\varphi. \tag{A1}$$

As a consequence, one has to change $\sin\varphi$ to $\cos\varphi$ in Eq. (7). Then due to the symmetry only the dipole moment along the x axis is created and no dipole moment along the y axis. When analyzing the matrix elements $\langle\psi_{k'}|\cos\varphi|\psi_k\rangle$ that determine the dynamics of $\mu_x(t)$, it is obvious that only transitions between states of the same parity are allowed. We find

$$\langle\psi_{k'}|\cos\varphi|\psi_k\rangle = \frac{1}{2}(\delta_{k,k'+1} + \delta_{k,k'-1}) \tag{A2}$$

if k and k' are integer (odd states) and

$$\langle\psi_{k'}|\cos\varphi|\psi_k\rangle = \frac{\chi(k')\chi(k)}{\pi}\left\{\frac{k-k'}{(k-k')^2-1}\sin[(k-k')\pi] + \frac{k+k'}{(k+k')^2-1}\sin[(k+k')\pi]\right\} \tag{A3}$$

if k and k' are noninteger (even states), where

$$\chi(a) = \left(\sqrt{1+\frac{\sin(2a\pi)}{2a\pi}}\right)^{-1}. \tag{A4}$$

From Eq. (A2) it follows that only the coherences between the neighboring levels contribute to the dynamics of the dipole moment in the case of odd states even though the coherences between distant levels can be excited by strong HCPs. In the case of even states also the matrix elements for transitions between distant states are different from zero. However, on one hand, the values of $k-k'$ and $k+k'$ are close to integer numbers for not very distant levels (see Fig. 2) and consequently $\sin[(k-k')\pi]$ and $\sin[(k+k')\pi]$ are close to zero for any impurity barrier strength. On the other hand, the coefficients of the sine functions in Eq. (A3) dictate vanishing transitions matrix elements for distant levels. Therefore contributions to the dynamics of the dipole moment of higher frequencies connected with transitions between distant levels are strongly suppressed as compared to the case when the HCP is polarized along the y axis, in which case the transitions between the states of different parity play a role and the transition matrix elements are given by

$$\langle\psi_{k_o}|\sin\varphi|\psi_{k_e}\rangle = -\frac{\chi(k_e)}{\pi}\frac{4k_e k_o\sin(k_e\pi)}{k_o^4+k_e^4-2(k_e^2+k_o^2)-2k_o^2k_e^2+1}, \tag{A5}$$

where k_e is related to an even state and k_o is related to an odd state. In general, only marginal differences in the time dependence of the generated charge polarization and the emission properties can be noticed compared to the case of a vanishing impurity barrier if the applied HCP is polarized along the x axis. The physical interpretation of this fact is that the contributions to the dipole moment and the corresponding electric fields from the electrons accelerated by the impurity potential at the left and the right sides of the ring compensate each other to high extent. This is a consequence of the symmetry of the ring and excitation.

APPENDIX B: TRANSITION COEFFICIENTS

The transition coefficients introduced in Eqs. (6) and (10) are

$$C_{k,k_0}^{\mathrm{odd,odd}} = -\frac{1}{4\pi}[\tilde{J}_{k+k_0}(\alpha) - \tilde{J}_{k-k_0}(\alpha) - \tilde{J}_{-k+k_0}(\alpha) + \tilde{J}_{-k-k_0}(\alpha)], \tag{B1}$$

$$C_{k,k_0}^{\mathrm{odd,even}} = \frac{i\chi(k_0)}{4\pi}[\tilde{J}_{-k-k_0}(\alpha)e^{-ik_0\pi} - \tilde{J}_{k-k_0}(\alpha)e^{-ik_0\pi} + \tilde{J}_{-k+k_0}(\alpha)e^{ik_0\pi} - \tilde{J}_{k+k_0}(\alpha)e^{ik_0\pi}], \tag{B2}$$

$$C_{k,k_0}^{\mathrm{even,even}} = \frac{\chi(k)\chi(k_0)}{4\pi}[\tilde{J}_{k+k_0}(\alpha)e^{-i(k+k_0)\pi} + \tilde{J}_{-k+k_0}(\alpha)e^{i(k-k_0)\pi} + \tilde{J}_{-k-k_0}(\alpha)e^{i(k+k_0)\pi} + \tilde{J}_{k-k_0}(\alpha)e^{i(-k+k_0)\pi}], \tag{B3}$$

$$C_{k,k_0}^{\mathrm{even,odd}} = \frac{i\chi(k)}{4\pi}[\tilde{J}_{-k-k_0}(\alpha)e^{-ik\pi} - \tilde{J}_{-k+k_0}(\alpha)e^{ik\pi} + \tilde{J}_{k-k_0}(\alpha)e^{ik\pi} - \tilde{J}_{k+k_0}(\alpha)e^{ik\pi}], \tag{B4}$$

where

$$\tilde{J}_m(\alpha) \equiv \int_0^{2\pi} e^{im\varphi}e^{i\alpha\sin\varphi}d\varphi. \tag{B5}$$

[1] Y. Aharonov and D. Bohm, Phys. Rev. **115**, 485 (1959).
[2] Y. Aharonov and D. Bohm, Phys. Rev. **123**, 1511 (1961).
[3] R. A. Webb, S. Washburn, C. P. Umbach, and R. B. Laibowitz, Phys. Rev. Lett. **54**, 2696 (1985).
[4] M. Buttiker, Y. Imry, and R. Landauer, Phys. Lett. **96A**, 365 (1983).
[5] M. Buttiker, Y. Imry, and M. Y. Azbel, Phys. Rev. A **30**, 1982 (1984).
[6] R. Landauer and M. Buttiker, Phys. Rev. Lett. **54**, 2049 (1985).
[7] D. Mailly, C. Chapelier, and A. Benoit, Phys. Rev. Lett. **70**, 2020 (1993).
[8] A. Fuhrer, S. Lüscher, T. Ihn, T. Heinzel, K. Ensslin, W. Wegscheider, and M. Bichler, Nature (London) **413**, 822 (2001).
[9] R. A. Webb, S. Washburn, and C. P. Umbach, Phys. Rev. B **37**, 8455 (1988).
[10] A. van Oudenaarden, Y. V. Nazarov, and J. E. Mooij, Phys. Rev. B **57**, 8816 (1998).
[11] Y. Imry, *Introduction to Mesoscopic Physics* (Oxford University Press, New York, 2002).
[12] J. Nitta, F. E. Meijer, and H. Takayanagi, Appl. Phys. Lett. **75**, 695 (1999).
[13] A. Lorke, R. J. Luyken, A. O. Govorov, J. P. Kotthaus, J. M. Garcia, and P. M. Petroff, Phys. Rev. Lett. **84**, 2223 (2000).
[14] W. Rabaud, L. Saminadayar, D. Mailly, K. Hasselbach, A. Benoit, and B. Etienne, Phys. Rev. Lett. **86**, 3124 (2001).
[15] L. W. Yu, K. J. Chen, J. Song, J. Xu, W. Li, X. F. Li, J. M. Wang, and X. F. Huang, Phys. Rev. Lett. **98**, 166102 (2007).
[16] A. Müller-Groeling and H. A. Weidenmüller, Phys. Rev. B **49**, 4752 (1994).
[17] Y. Liu, Phys. Lett. A **241**, 184 (1998).
[18] M. Mosko, P. Vagner, A. Gendiar, and R. Nemeth, Physica B **378-380**, 908 (2006).
[19] H.-M. Li and J.-L. Xiao, Physica B **396**, 91 (2007).
[20] A. Matos-Abiague and J. Berakdar, Phys. Rev. Lett. **94**, 166801 (2005).
[21] A. S. Moskalenko, A. Matos-Abiague, and J. Berakdar, Phys. Rev. B **74**, 161303(R) (2006).
[22] A. S. Moskalenko, A. Matos-Abiague, and J. Berakdar, EPL **78**, 57001 (2007).
[23] Y. V. Pershin and C. Piermarocchi, Phys. Rev. B **72**, 245331 (2005).
[24] Y. V. Pershin and C. Piermarocchi, Phys. Rev. B **75**, 035326 (2007).
[25] I. Barth, J. Manz, Y. Shigeta, and K. Yagi, J. Am. Chem. Soc. **128**, 7043 (2006).
[26] Z.-G. Zhu and J. Berakdar, Phys. Rev. B **77**, 235438 (2008).
[27] R. Warburton, C. Schaflein, D. Haft, F. Bickel, A. Lorke, K. Karrai, J. Garcia, W. Schoenfeld, and P. Petroff, Nature (London) **405**, 926 (2000).
[28] M. Bayer, M. Korkusinski, P. Hawrylak, T. Gutbrod, M. Michel, and A. Forchel, Phys. Rev. Lett. **90**, 186801 (2003).
[29] A. Matos-Abiague and J. Berakdar, Phys. Rev. B **70**, 195338 (2004).
[30] P. B. Corkum and F. Krausz, Nat. Phys. **3**, 381 (2007).
[31] R. Kienberger *et al.*, Science **297**, 1144 (2002).
[32] P. Paul, E. Toma, P. Breger, G. Mullot, F. Auge, P. Balcou, H. Muller, and P. Agostini, Science **292**, 1689 (2001).
[33] M. Lewenstein, P. Balcou, M. Y. Ivanov, A. LHuillier, and P. B. Corkum, Phys. Rev. A **49**, 2117 (1994).
[34] P. Antoine, A. L'Huillier, and M. Lewenstein, Phys. Rev. Lett. **77**, 1234 (1996).
[35] Y. Mairesse *et al.*, Science **302**, 1540 (2003).
[36] D. You, R. R. Jones, P. H. Bucksbaum, and D. R. Dykaar, Opt. Lett. **18**, 290 (1993).
[37] R. R. Jones, D. You, and P. H. Bucksbaum, Phys. Rev. Lett. **70**, 1236 (1993).
[38] S. Park, A. Weiner, M. Melloch, C. Siders, J. Siders, and A. Taylor, IEEE J. Quantum Electron. **35**, 1257 (1999).
[39] C. M. Dion, A. B. Haj-Yedder, E. Cancès, C. Le Bris, A. Keller, and O. Atabek, Phys. Rev. A **65**, 063408 (2002).
[40] D. Daems, S. Guerin, H. R. Jauslin, A. Keller, and O. Atabek, Phys. Rev. A **69**, 033411 (2004).
[41] The frequency $\Omega_0=\hbar/(m^*\rho_0^2)$ is related to the global energy scale set by the system size. The energy scale set by the Fermi energy enters ω_0 through the particle number N because the ring is isolated. As experimentally demonstrated, the emission can be charge tuned to be in the optical range [27].
[42] A. W. Clark, A. Glidle, D. R. S. Cumming, and J. M. Cooper, Appl. Phys. Lett. **93**, 023121 (2008).
[43] R. Hubner and R. Graham, Phys. Rev. B **53**, 4870 (1996).
[44] A. S. Moskalenko and J. Berakdar, Phys. Rev. A **78**, 051804(R) (2008).
[45] G. Piacente and G. Q. Hai, J. Appl. Phys. **101**, 124308 (2007).
[46] W. C. Tan and J. C. Inkson, Phys. Rev. B **60**, 5626 (1999).
[47] T. Chakraborty and P. Pietiläinen, Phys. Rev. B **50**, 8460 (1994).
[48] A. Bertoni, M. Rontani, G. Goldoni, and E. Molinari, Phys. Rev. Lett. **95**, 066806 (2005).
[49] N. Jukam and M. S. Sherwin, Appl. Phys. Lett. **83**, 21 (2003).
[50] X. Xie, A. Scrinzi, M. Wickenhauser, A. Baltuška, I. Barth, and M. Kitzler, Phys. Rev. Lett. **101**, 033901 (2008).
[51] Recently, high harmonics generation has been demonstrated theoretically for a ring-shaped potential of molecular rings [50].